IOSR Journal Of Applied Physics (IOSR-JAP)
e-ISSN: 2278-4861.Volume 15, Issue 5 Ser. I (Sept. – October. 2023), PP 01-09
www.Iosrjournals.Org

Chemical Synthesis, Structural, And Optical Characterization Of Mg Sm_x Zn $Fe_{2-X}o_4$ Nanoparticles And Applications

G. Koteswari[1], N. Hari Kumar[2*], D. Ravinder[1*]
[1]Department Of Physics, University College Of Science, Osmania University, Hyderabad, India-500007.
[2]Department Of Physics, St. Mary's Group Of Institutions, Deshmukhi, Yadadri Bhongiri, India-508116.

Abstract
In the present work Sm^{3+} substituted Mg-Zn ferrites synthesised by Citrate Gel Auto- Combustion method and range of 0.000 to 0.0030 (X step of 0.0005). X-ray diffraction (XRD), field emission scanning electron microscopy (FE-SEM), UV-vis investigation and, fourier-transformed infrared spectroscopy (FTIR). The XRD and SEM images indicate nanoscale ranges as well as the cubic spinel structure, which is merely phased, and confirm the normal crystallite size. The lattice parameter and volume decrease as density increases. The FTIR data clearly suggests that two metallic bands have formed, confirming the cubic spinel ferrites. The UV-vis investigation demonstrates that the calculated direct band gap energy values have a violet shift. They are excellent for water purifications, memory storage devices.

Keywords*: Chemical synthesis: Nano particle: Structural characterization: Optical studies.*

Date of Submission: 26-08-2023 Date of Acceptance: 06-09-2023

I. Introduction

The general formula for Nano spinel ferrites is AB_2O_4 wherein "A" are divalency metal ions similar like Zn^{2+}, Ni^{2+} and Co^{2+} and "B" are having tri-valency metallic ion Fe^{3+}, Sm^{3+}, Sm^{3+}, La^{3+}, Al^{3+} etc. it contains a significant category of magnetic substances having numerous uses in storage, microwave, magnetic diagnostic equipment including magnetic drug delivery etc. [1]. The substances get crystallized to cubic closely packed spinel structure of "O" ion. The cations fill up dual kinds of interstitial places or sites or positions called Tetrahedral or Octahedral. Sites: A-Tetrahedral, B-Octahedral occupancy of these positions is many times depicted using chemical method "($[A^{2+}{}_{1-\delta}Fe^{3+\delta}]$ $[A^{2+\delta}Fe^{3+}{}_{2-\delta}]$ $O^{2-}{}_4$)" everywhere the parentheses and the square brackets signify A, B site correspondingly, "A" signifies a cation of valency as two and δ is inversion parameter [2]. The production of spinel ferrite nanoparticles has newly gained a Plenty of focus, and the fundamental effect of the preparation circumstances on the structural and physical properties of the ferrites is investigated [3].

The as-prepared material was then characterised using various techniques such as structural, SEM, FTIR and UV spectra. The current work aims to evaluate how Sm^{3+} ion doping impacts the structural and optical properties of Mg-Zn spinel ferrites, as well as whether they are suitable for water purifications, memory storage devices.

II. Sample preparation

The selected sample is samarium substituted magnesium, zinc ferrites, have been synthesized by using citrate--gel auto--combustion practice. The chemical formulae for series are as fallows. $MgSm_xZnFe_{2-x}O_4$ 0.000 to 0.0030 (X step of 0.0005).

Raw materials and apparatus required for the synthesis of the prepared and the essential quantity of individual nitrate was weighted by calibrated electronic balance with an accuracy of 10^{-4} grams for each compound. The amount of metal nitrates after calculation defined in the raw constituents of a specific nano-ferrite system along with citric acid were dispersed in a least required amount of double distilled water. The mixture was made to undergo thorough stirring using magnetic stirrer to get homogenized solution.The solution of "citric acid" taken as fuel due to its superior complexing characteristics. We take a constant ratio as 3:1 for citric acid to metal nitrate for every specimen.Then we formulate the nitrate-citrate solution to which NH_3 solution is added by the drop to keep a constant P^H of 7 after which mixing and heating of solution by constantly stirring until 100ºC temperature is reached for 10 to 12 hrs. resulting in the formation of a viscous gel. Once more evaporating the water contained in the mixture resulting in the formation of powder.

This favorable ferrite powder specimen is exposed to 500˚C for 4 hours and then analyzed using X-ray Diffraction, Scanning Electron Microscopy: SEM, Fourier Transform - Infrared Spectroscopy: FT-IR and then Energy Dispersive Xray Spectroscopy.

III. Characterization Techniques

The structurally characterizing the prepared ferrite specimens was undertaken through XRD with Cu-Kα (λ=1.405A^{o}) radiation measured at room normal temperature through constant slow skim through in the array range of 10˚ to 80˚ to learn the phase, structure and crystalline size. The typical grain size and surface morphology of the prepared Co-Er and Co-Zn-La nano ferrites by SEM:Scanning Electron Microscope and their average particle size dimensions were carried out using TEM:Transmission Electron Microscope and AFM.

Energy Dispersive Spectrometer was used to conduct elemental analysis. FTIR absorption spectra of investigated nano ferrites powder (pellets are in KBr) were measured by FTIR:Fourier Transform Infrared Spectrophotometer ranging between (400 to 1000 cm$^{-1)}$ with a resolve of (1 cm^{-1}).

IV. Result and Discursion

XRD Analysis of Sm^{3+} substituted Mg-Zn nanoferrrites

The D and an of the samples utilised in this study are shown in Figure 1 and Table 1. The higher lattice constant of $MgSm_xZnFe_{2-x}O_4$ could be attributed to the larger ion radius change between Sm^{3+} and Fe^{3+}, as illustrated in Fig. 1. When Mg^{2+} ions are replaced, lattice distortion between Sm^{3+} and Fe^{3+} is more likely because to the higher ion range change, resulting in larger lattice constants [4-6]. Concurrently, crystal size comparison results indicate that $MgSmxZnFe_{2-x}O_4$ develops smaller grains than under the same experimental conditions, which may be attributed to the former's greater lattice distortion. It is possible that replacing these ions increases perovskite phase production while inhibits spinel phase growth. Furthermore, as the atomic number increases, so does the decreases size of the crystal. Table 1 offers information about certain powders generated during auto combustion, as well as additional replacement factors' lattice constants and statistics. The crystalline size has shrunk, indicating that crystal lattice decreases and crystal development occurred during the subsequent boiler phase, resulting in a more complete crystal [7-9]. Furthermore, increasing the proportion of citric acid can reduce crystal size, which is consistent with published research findings.

When Sm^{3+} is doped, the sample formed after combustion has a smaller crystal size, indicating that the crystal expands during the subsequent heating progression; a sample obtained after burning has a low lattice constant in some cases. indicating that the lattice may increase during the next heating system procedure, which may be related to Sm^{3+} ion translocation [10-12].

$Mg\,Sm_xZnFe_{2-x}O_4$	M. W (gm/ml)	Crystallite size (nm)	Lattice constant (Å)	XRD Density(d_x) (gm/cc)	Volume (Å)^3
X = 0.000	201.01	32.14	8.19	0.6490	521.01
X = 0.0010	203.05	29.99	8.05	0.6010	515.22
X = 0.0015	206.66	29.10	8.00	0.5910	500.50
X = 0.0020	208.10	28.25	7.98	0.5818	499.16
X = 0.0025	210.10	27.45	7.56	0.5712	498.45
X = 0.0030	212.12	26.22	7.19	0.5311	486.50

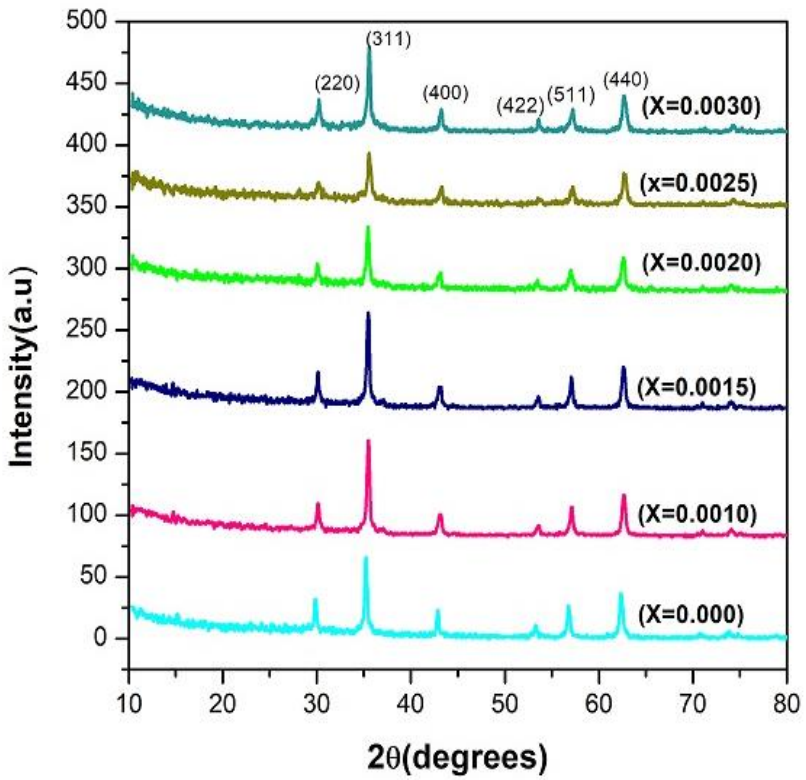

Fig. 1. XRD graph of MgSmxZnFe$_{2-x}$O$_4$ spinel ferrite samples.

FE-SEM Analysis of Sm^{3+} substituted Mg-Zn nanoferrrites.

The external syllable structure of MgSmxZnFe2$_{-x}$O$_4$ nanoparticles (X = 0.000, 0.0010, 0.0015, 0.0020, 0.0025, and 0.0030) was investigated by FE-SEM. The FESEM pictures are shown in Figure 2. The clusters of grains were clearly identified in the material. In the instance of the specimen, highly interacting granules were discovered. This pattern could be explained by the substantial magnetic interactions between the grains [13-15]. However, the substance produced a few round stones resembling grains with a few aggregated granules. Aside from that, the current materials' grain size was established utilising the rectilinear seize technique [16-18]. The

results for Mg Sm_x Zn $Fe_{2-x}O_4$ materials ranged between 41 and 56 nm. It could be due to considerable magnetic NP aggregation [19].

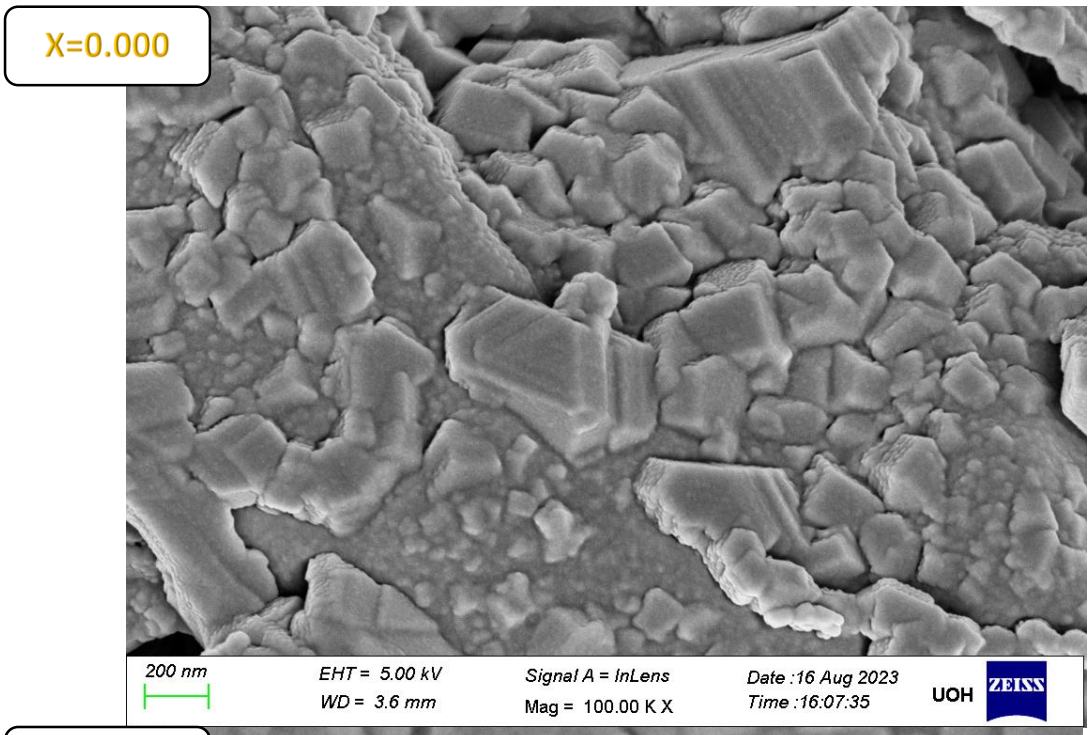

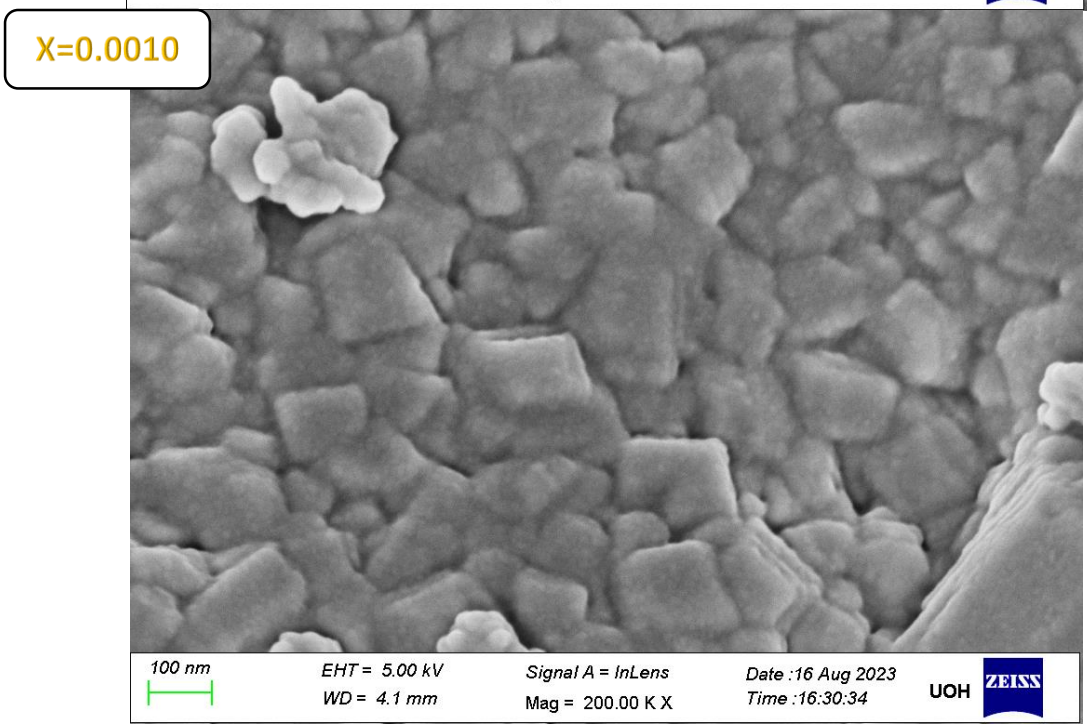

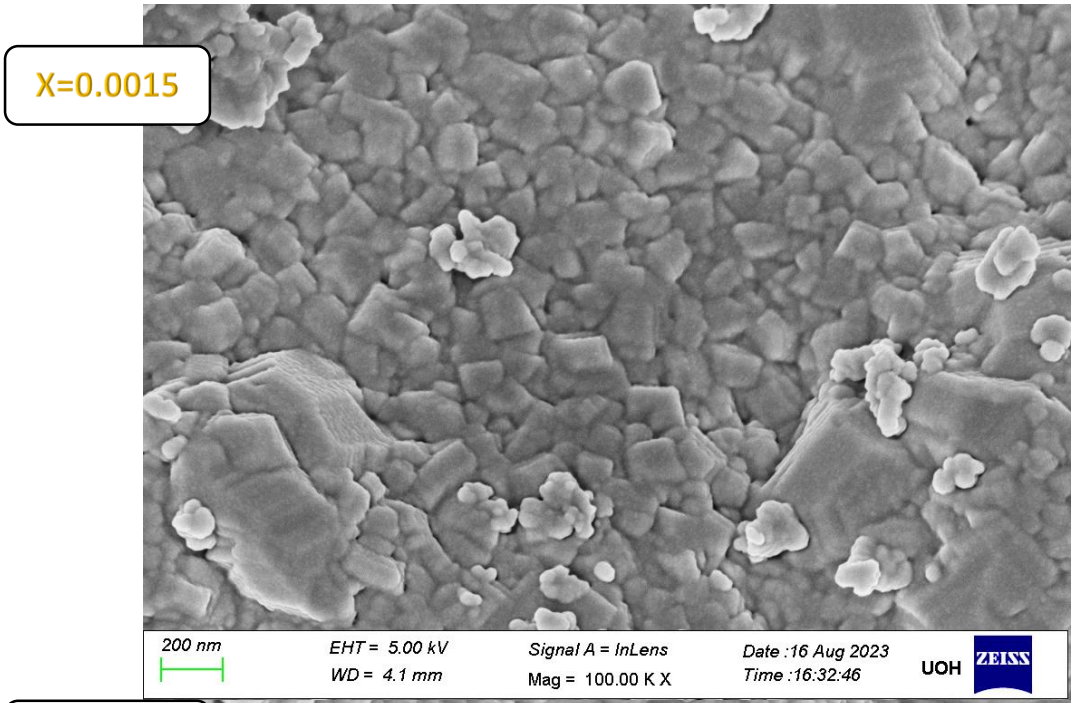
X=0.0015
200 nm
EHT = 5.00 kV
WD = 4.1 mm
Signal A = InLens
Mag = 100.00 K X
Date :16 Aug 2023
Time :16:32:46
UOH
ZEISS

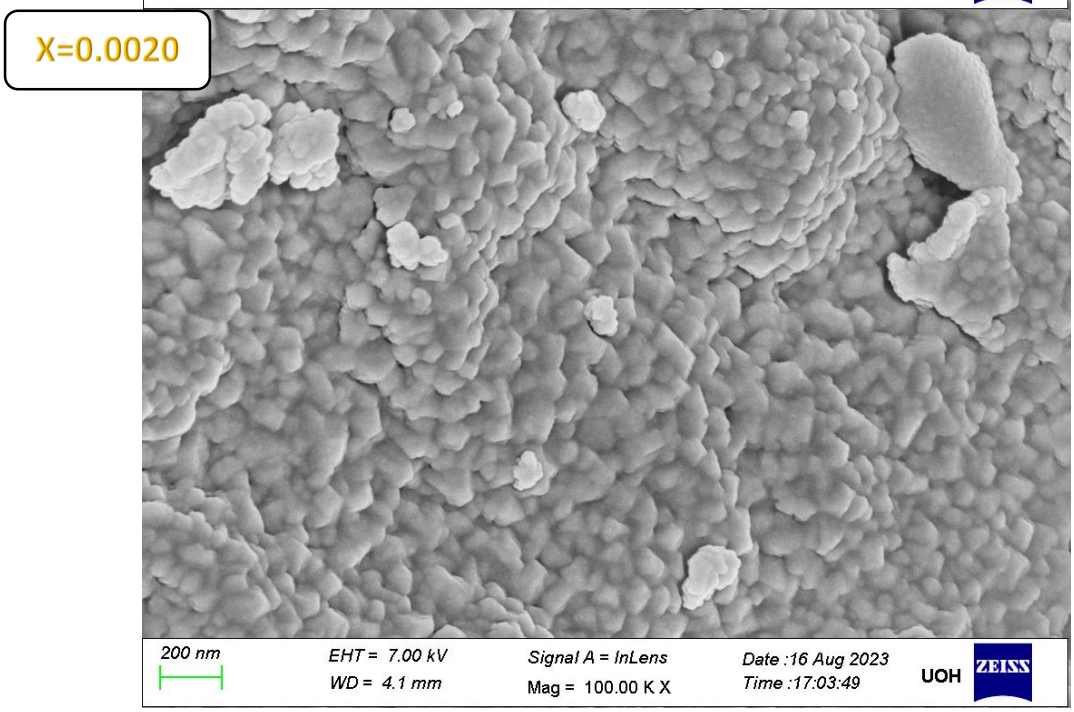
X=0.0020
200 nm
EHT = 7.00 kV
WD = 4.1 mm
Signal A = InLens
Mag = 100.00 K X
Date :16 Aug 2023
Time :17:03:49
UOH
ZEISS

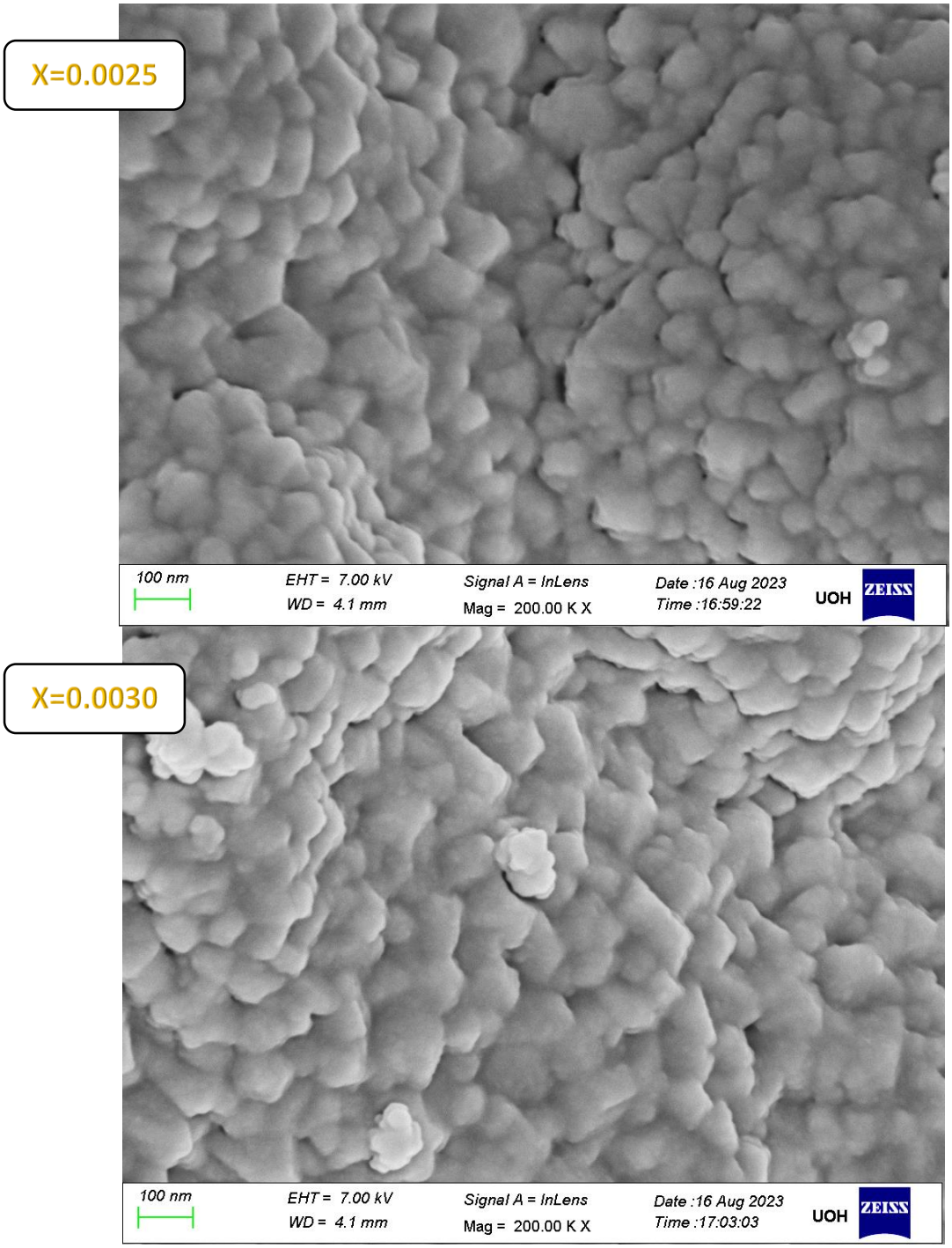

Fig. 2. SEM graph of $MgSmxZnFe_{2-x}O_4$ spinel ferrite samples.

Fourier-transformed infrared spectroscopy (FTIR) Analysis of Sm^{3+} substituted Mg -Zn nanoferrrites.

To evaluate the spinel structure and explore the chemical properties of ferrite, IR spectroscopy of Sm^{3+} doping Mg-Zn ferrite was done. Two primary absorption bands may be recognised between 400 and 640 cm^{-1}. Overall, the wide-ranging region represents the tetra A-site's vibrational frequencies (v_1 and v_2), and the thin band represents the octahedral B-sites [20-22]. FTIR spectrum analysis is frequently used to provide the cation distribution between A and B-sites. In the $MgSm_xZnFe_{2-x}O_4$ trial shown in Fig. 3, the Sm^{3+} cations are more likely than the A-site cations to substitute the Fe^{3+} ions at the B-site. As a result, the substituted ferric ions at B can make their way to A. Furthermore, vibrational frequencies of 1545 cm-1 and 2359.3 cm^{-1} are associated with Mg-O, Fe-O (A-site) and Mg-O, Fe-O, Sm-O (B-site) [23]. Similarly, in the case of $MgSm_xZnFe_{2-x}O_4$ material stretching vibrations [24-25]. This means that cations are spread across the two spinel structural locations was shown in Table 2.

The tetra and octal absorbent bands become less frequent as Sm^{3+} doping rises. These modifications are linked to the range of doped ions as well as the reordering of Mg^{2+} and Fe^{3+}. Sm^{3+} ions tend to occupy the B-sites due to their wide radius. For the time being, the Mg^{2+} ion has a greater ionic radius (1.72) than the Fe^{3+} ion (0.67). Because Sm^{3+} ions are found in B-sites, some Mg^{2+} ions migrate to A-sites, and a tiny amount of Fe^{3+} ions migrate from A-sites to B-sites to relieve stress [26]. when a result, when the number of Mg^{2+} ions in A-sites increases, so do their ionic radii. Similarly, increasing the amount of Sm^{3+} ions in the ionisation radii of the B-sites is beneficial.

The tetrahedral band frequency (v_1) for typical samples in our study is shown in Table 2. The table shows how Fe^{3+} ions differ from Sm^{3+} substituted Fe^{3+} ions. The variance in band positions is due to a variation in the Fe^{3+}-O^{2-} distance [27-30]. This study shows that when Sm^{3+} substituted Mg^{2+} ions and Sm^{3+} substituted Fe^{3+} ions are present, ion rearrangement occurs. However, the first scenario results in more Mg^{2+} ions entering the B site from the A site, producing A site constriction.

Mg SmxZnFe2$_{-x}$O$_4$	Absorption band frequencies(cm^{-1})	
	υ_1	υ_2
X = 0.000	525.45	319.0
X = 0.0010	532.10	300.1
X = 0.0015	535.45	298.5
X = 0.0020	537.10	288.4
X = 0.0025	539.81	275.5
X = 0.0030	540.00	262.4

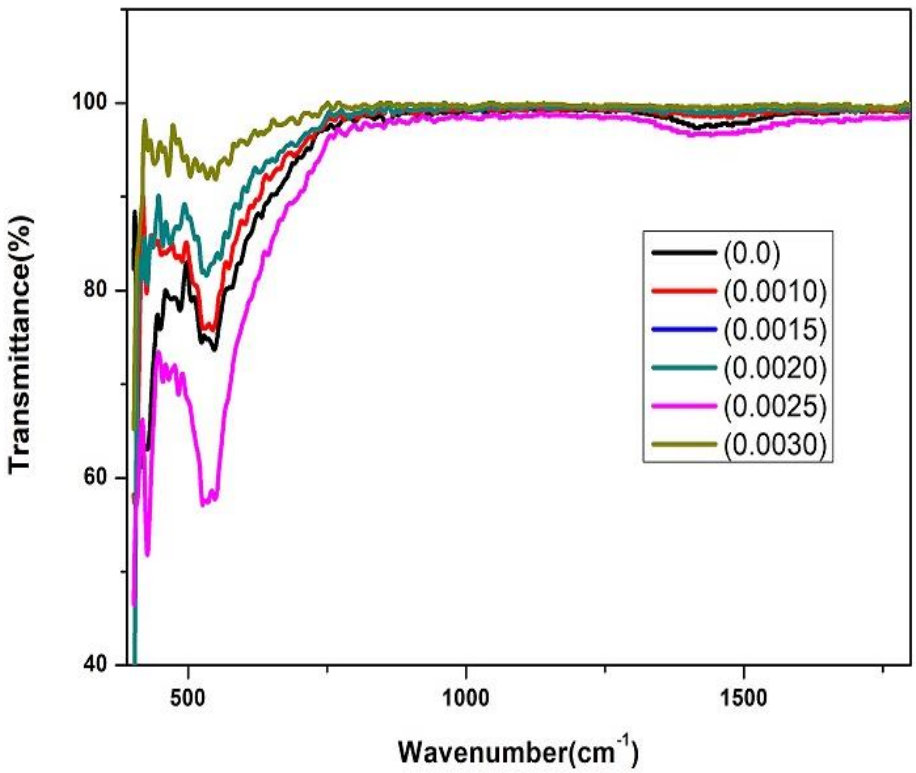

Fig. 3. FTIR graph of MgSmxZnFe$_{2-x}$O$_4$ spinel ferrite samples.

Optical investigation Analysis of Sm^{3+} substituted Mg-Zn nanoferrrites

Figure 4 depicts the absorption spectrum of a material in the wavelength range of 200-800 nm. Significant absorption in this region is characterised by the presence of four absorption bands for each component. These absorption bands represent two types of transitions: inter-band and intra-band transitions [31-33]. The optical band gap altitude (Eg) is represented by the gap energy (Eg) in Table 3.

The O-3p orbital, which operates similarly to the valence band, and the d orbital, which serves as the conduction band, define the band configuration of a Mg Sm_x Zn $Fe_{2-x}O_4$ ferrite. The O-3p level up to the Fe-4d level is thought to be the source of electron excitation in the Mg Sm ferrite, which accounts for the visible light

absorption spectra [34-36]. The composition has been shown to change the location of the absorption bands. The already known compounds, due to their high band gaps [37-39].

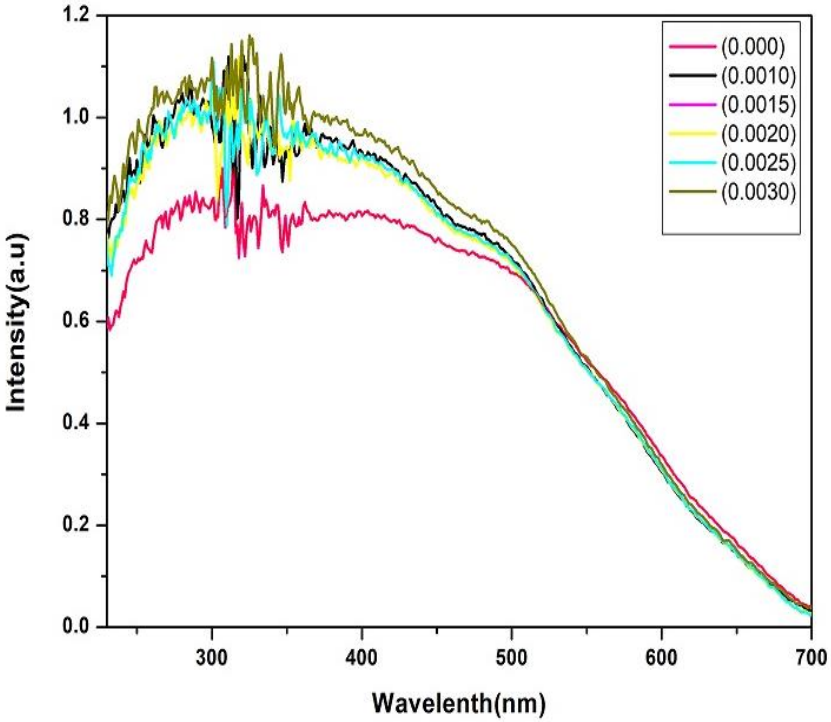

Fig. 4. UV graph of $MgSmxZnFe_{2-x}O_4$ spinel ferrite samples.

Table 3. UV parameters of the prepared Sm substituted Mg-Zn nano ferrite sample

Mg $SmxZnFe2_{-x}O_4$	Band gap(eV)
X = 0.000	433.21
X = 0.0010	413.10
X = 0.0015	392.10
X = 0.0020	389.19
X = 0.0025	379.45
X = 0.0030	360.99

V. Conclusions

The Sm^{3+} substituted Mg-Zn ferrites synthesised by Citrate Gel Auto- Combustion method. This method is more efficient, conveniently and economically used to obtain a homogenized nano-sized mixed ferrite. The main objective of the present studies of samarium substituted magnesium Zink nano ferrites chemical formulas Mg Sm_x Fe_{2-x} O $_4$ nanoparticles (X = 0.000, 0.0010, 0.0015, 0.0020, 0.0025, and 0.0030) nanoparticles. The preparation method of Citrate Gel Auto-Combustion is to be an alternative to get nano size powder. XRD pattern of the Sm^{3+} substituted Mg-Zn ferrites samples having the single phase cubical spinal structure. Ferrite's composition of Mg Sm_x Fe_{2-x} O_4 chemical composition of the sample's crystallite size is between 26 to 32 nm. Doping Sm^{3+} substituted ferrite system decreases the lattice parameter and XRD density. The Structural morphology was similar for Sm^{3+} substituted all prepared particles. It's confirmed from the SEM Micrograph and They are largely collections. Formation of v_1 and v_2 fundamental bands formed from FTIR spectrum corresponding to octahedral and tetrahedral sites in the nano ferrite structure. Optical studies by UV–DRS decrease in wavelength with increase in Sm^{3+} concentration. The absorption edge shifts from 360nm to 433 nm.

Acknowledgment

The authors wish to express their appreciation to SV TTD, HOD & BOS of the Department of Physics, University College of Science. OU, Hyderabad.

References

[1] K D Martinson Et Al. J. Alloys Compd. 894 162554 (2022)
[2] Vivekdhand, Hyunhoshin, Gyeonghunhan, S Bharadwaj, Kyongyoprhee And Sanghoonkim J. Alloys Compd. 910, 164765 (2022)
[3] V Ludhiya, D Ravinder And A Edukondalu Inorg Chem Commun. 150 110558 (2023)
[4] Banoth Baburao, N Hari Kumar, Avula Edukondalu, M Venkata Narayana And D Ravinder Inorg. Chem. Commun. 148 110355 (2023).
[5] A Sadaqat Et Al. Ceram. Int. 45 22538 (2019)
[6] Aleksandra Rękorajska Et Al. Chem Nano Mat. 4 2 (2017)
[7] D D Andhare, S R Patade And S A Jadhav Appl. Phys. A. 127 480 (2021)
[8] Asma Aslam Et Al. J Phys Chem Solids.154 110080 (2021)
[9] Muhammad Junaid Et Al. J. Magn. Magn. Mater. 419 338 (2016)
[10] Adil Murtaza Et Al. Physica, B, Condens. Matter. 646 414287 (2022)
[11] Kiran Naz Junaid Et Al. Mater Chem Phys. 285 126091 (2022)
[12] S L Galagali, R A Patil, R B Adaki And C S Hiremath Int. J. Self-Propagating High-Temp. Synth. 27 107 (2018)
[13] N Hari Kumar, D Ravinder And A Edukondalu J. Chem. Phys. 81 171-180 (2022)
[14] Edapalli Sumalatha, N Hari Kumar, Avula Edukondalu, D Ravinder Inorg. Chem. Commun. 146 110200 (2022).
[15] R Panda, R Muduli, G Jayarao, D Sanyal And D Behera J. Alloys Compd. 669 19 (2016)
[16] A M Kumar, M C Verma, C L Dube, K H Rao And S C Kashyap J. Magn. Magn. Mater. 8 047801 (2018)
[17] Y J Yang, C I Sheu, S Y Cheng And H Y Chang J. Magn. Magn. Mater. 284 220 (2004)
[18] P. Jain And O. Subohi J Supercond Nov Magn. 35 291 (2022)
[19] N Venkatesh, N Hari Kumar, S Goud, D Ravinder, P V. Somaiah, T A. Babu, N.V.K. Prasad Biointerface Res. Appl. Chem. 11 15037–15050 (2021)
[20] A Tokkaya, S K Çetin And B Altan J Supercond Nov Magn. 35 303 (2022)
[21] N H. Kumar, D. Edukondalu, D Ravinder Chin. J. Phys. 81 171–180 (2023)
[22] Yatin P Desai, Shantadurga Desai, Disha Sinai Sangaonkar, Manoj M Kothawale And G K Naik Mater. Today: Proc. 46 2261 (2021)
[23] N H. Kumar, D Ravinder, A Edukondalu Appl. Phys. A 128 978 (2022).
[24] N Maramu Et Al. J Mater Sci: Mater Electron 32 10376 (2021).
[25] Arminder Kaur And Gagan Kumar Bhargava Mater. Today: Proc. 37 3082 (2021)
[26] Ayman Galal, Olfat Sadek, Moataz Soliman, Shaker Ebrahim And M Anas Sci Rep. 11 20170 (2021)
[27] Majid Niaz Akhtar Et Al. Ceram. Int. 47 11878 (2021)
[28] N Hari Kumar, D Ravinder, T Anilbabu, Nakiraboina Venkatesh, S Swathi, N V. Krishna Prasad Journal Of Indian Chemical Society 99 100362 (2022)
[29] H R Sharma, K M Batoo And P Sharma J Mater Sci: Mater Electron. 33 7528 (2022)
[30] C Murugesan Et Al. J. Magn. Magn. Mater. 550 169066 (2022)
[31] Bablu Chandra Das, F Alam And A K M Hossain Akther J Phys Chem Solids 142 109433 (2020)
[32] M Willander And Suresh Jain Academic Press, Imprint Of Elsevier, Publisher: Zd Oe Kruze, 74 322 (2023)
[33] B Aparna, A Edukondalu, D Ravinder, K A. Jaleeli Results In Chem. 5 100957 (2023)
[34] M M Arman J Supercond Nov Magn.35 1241 (2022)
[35] S J Kashyap, R Sankannavar And G M Madhu J Supercond Nov Magn. 35 2107 (2022)
[36] Xiyao, Jian Pingzhou, Xiao Lizhang And Xiao Mingchen J. Magn. Magn. Mater. 550 169099 (2022)
[37] N. Hari Kumar, D Ravinder, A Edukondalu Appl. Phys. A. 128 978 (2022).
[38] O Michael And Ogunbunmi Andre M Strydom J. Alloys Compd. 895 162545 (2022)
[39] B Baburao, N Hari Kumar, A Edukondalu, D Ravinder Braz J Phys 53 91 (2023)